ARTICLE OPEN

Check for updates

Corrosion inhibition at emergent grain boundaries studied by DFT for 2-mercaptobenzothiazole on bi-crystalline copper

Fatah Chiter[1]✉, Dominique Costa[1], Vincent Maurice[1]✉ and Philippe Marcus[1]✉

Inhibition of the initiation of intergranular corrosion was modeled at the atomic scale for 2-mercaptobenzothiazole (MBT) adsorbed on a (110)-oriented copper bi-crystal exposing an emergent Σ9 coincident site lattice (CSL) grain boundary (GB) using dispersion-corrected density functional theory (DFT-D). At both isolated molecule and full, dense monolayer coverages, the molecule adsorbed on the grain and GB sites stands perpendicular or tilted with no parallel orientation to the surface being favored. Chemical bonding of the thione and thiolate conformers involves both S atoms or the exocyclic S and N atoms, respectively. The full, dense monolayer is formed with a net gain in energy per surface area, but at the cost of a significant molecule deformation. It significantly enhances the Cu vacancy formation energy at the grain and GB sites, revealing that MBT also inhibits Cu dissolution for the more susceptible GBs with efficiency depending on atomic density of GB emergence.

npj Materials Degradation (2023)7:5 ; https://doi.org/10.1038/s41529-022-00314-5

INTRODUCTION

Grain boundaries (GBs) play a crucial role for the durability of metallic materials. Their emergence at polycrystalline surfaces provides preferential atomic sites for the initiation of intergranular corrosion, which, if not mitigated by corrosion inhibitors or formation of a passivating surface oxide, propagates into the subsurface region and eventually leads to the microstructure failure. We recall that according to the misorientation angle, grain boundaries (GBs) can be categorized into low-angle (<15°) and high-angle (>15°) GBs. The latter contain two classes: (i) coincidence site lattices (CSL) boundaries denoted by a Σn index, where n^{-1} refers to the fraction of lattice sites shared by the two crystals at the interface, and (ii) random boundaries that cannot be described by a coincidence site lattice (see ref. [1] and references therein). Some CSL boundaries are also called "special boundaries" when they have comparatively lower reactivity, owing to their lower boundary energy, than random or other CSL boundaries. According to the specific GB plane orientation, Σ3 twins can be coherent or incoherent. Σ3 coherent twins have GB plane of {111} orientation. Recently, the initiation of intergranular corrosion at various types of emergent GBs was studied at the nanometer scale on microcrystalline copper[2]. In situ Electrochemical Scanning Tunneling Microscopy (ECSTM) combined with Electron Back-Scatter Diffraction analysis of the same local GB regions demonstrated that the initiation of intergranular dissolution is dependent on the grain boundary character in acidic conditions in which copper does not passivate. It was found that random high-angle boundaries as well as Σ9 coincidence site lattice (CSL) boundaries are susceptible to the initiation of intergranular corrosion whereas Σ3 coherent twins with low-angle deviation are resistant in the same testing conditions.

The use of corrosion inhibitors is an effective approach to mitigate the corrosion of metals and alloys in contact with aggressive environments. On copper, numerous studies have been carried out for a better understanding of the surface interaction with corrosion inhibitors, as well as the inhibition mechanisms (see ref. [3] and references therein). Azole derivatives, such as 2-mercaptobenzothiazole (MBT, $C_7H_5NS_2$), form protective barrier layers in neutral, acidic, or alkaline conditions and are often used as corrosion inhibitors for copper or its alloys[4–16]. Recently, the adsorption of MBT on metallic and pre-oxidized Cu(111) model surfaces has been investigated, both experimentally and theoretically. It was shown that MBT adsorbs on metallic and pre-oxidized copper and forms organic multi-layers thereon[17–19]. DFT calculations also revealed that these molecules are able to heal local de-passivated zones exposing the bare metal next to the protecting oxide[20], with similar adsorption behavior than 2-Mercaptobenzimidazole (MBI) molecule[21,22]. On Cu(110), DFT calculations showed that MBT forms a dense monolayer on the surface, and increases the energy required for extracting Cu atoms from the surface, confirming that MBT adsorption inhibits Cu dissolution[23]. Indeed, experimental works have demonstrated that MBT is an anodic inhibitor in acid (pH = 2) and alkaline (pH = 13) aqueous solutions[1,24]. In HCl acid solution, MBT blocks the Cu(I) active dissolution in an overpotential range of 0.15–0.2 V[1]. Local ECSTM analysis showed the mitigation of net intergranular dissolution by the pre-adsorbed MBT surface layer but also revealed the local accumulation of reaction products in the GB regions. Low Σ CSL boundaries were observed to be protected by the pre-adsorbed MBT layer against net preferential dissolution whereas high Σ CSLs and random GBs were observed to react preferentially when compared to grains. For these intrinsically more reactive boundaries, net dissolution, mitigated by the MBT layer, was observed concurrently with protection resulting from preferential formation of reaction products in the GB regions. In alkaline media of NaOH studied in order to test different environments, MBT surface layers pre-formed after reductive dissociation of the native oxide, were observed to block the formation of a Cu(I) surface oxide and thus passivation, but to not entirely suppress residual reactivity[24]. Local ECSTM analysis confirmed a residual intergranular reactivity except for coherent twins. On CSLs and random boundaries, residual dissolution with accumulation of corrosion products or residual passivation was observed, depending on the barrier effect of the pre-formed

[1]PSL University, CNRS—Chimie ParisTech, Institut de Recherche de Chimie Paris/Physical Chemistry of Surfaces Group, 11 rue Pierre et Marie Curie, 75005 Paris, France.
✉email: fatah.chiter@chimieparistech.psl.eu; vincent.maurice@chimieparistech.psl.eu; philippe.marcus@chimieparistech.psl.eu

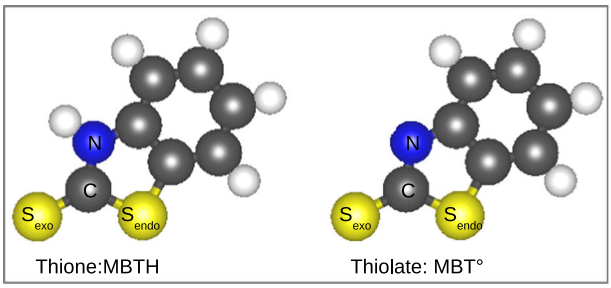

Fig. 1 Isolated MBT molecule under the thione (MBTH) and thiolate (MBT°) species. Color atoms correspond to Yellow: sulfur atoms, Blue: nitrogen, Gray: carbon, White: hydrogen.

inhibitor layer on oxide formation. For more reactive high Σ CSLs and random boundaries, pre-adsorbed MBT forms a barrier against passivation by oxide growth.

Here, we report DFT calculations that bring atomic-scale insight on how the MBT corrosion inhibitor may protect preferred local zones of dissolution corresponding to emergent grain boundaries, exposed in acidic and alkaline aqueous solutions where the surface oxide was reduced by cathodic reduction[1,24]. We examine in details the adsorption of the thione and thiolate conformers (see Fig. 1) of MBT on a (110)-oriented copper bi-crystal exposing a Σ9(2$\bar{2}$1)[110] 38.9° CSL grain boundary whose surface emergence is susceptible to the initiation of intergranular corrosion as shown previously[2]. We discuss the structure and energetics of the adsorption configurations as well as the energy required for extracting Cu atoms from the surface. This defect formation energy is directly related to the dissolution probability of one given Cu surface atom, and thus a relevant indicator of local corrosion susceptibility.

RESULTS AND DISCUSSION

Construction of the bi-crystal model

The model of an emergent Σ9(2$\bar{2}$1) [110] 38.9° GB was constructed using the CSL method, a construction method widely used and providing reasonable GB models[25–28]. The Cu(110) bi-crystal model was obtained from the fcc crystal structure, considering the [110] misorientation axis and a 38.9° misorientation angle to generate the grain boundary. We first optimized the bulk bi-crystal containing two oppositely oriented Σ9 GBs. Then we built a slab using the supercell shown in Fig. 2 with lateral dimensions: $x = 7.42$ Å in [$\bar{1}$14] direction and $y = 21.19$ Å in [2$\bar{2}$1] direction.

In the z [110] direction, the slab alternates six atomic layers with 18 and 16 atoms per unit cell. The layers with 18 atoms have an atomic density equal to that of the ideal (110) surface, those with 16 atoms have a lower atomic density in the GB region, due to the elimination of the redundant atoms. The periodic images of the slab in the [110] direction were interspaced by more than 18 Å of vacuum in order to minimize the interactions between them. As the model alternates metal layers with different atomic density, we considered two surface terminations to study the molecule/surface interaction. The two surface terminations are noted T_1 and T_2 for the high and low atomic surface density, respectively. They are shown in Fig. 3 with the variety of reactive sites within and near the GB plane labeled a to f. The terminations are in good agreement with the structures considered to study the segregation of P and S atoms impurities[29]. The Σ9 GB is chosen because it occurs frequently in fcc Cu[30–32] and its surface termination exposes a variety of reactive sites.

Previous investigation of the single-crystalline Cu(110) surface showed that the MBT molecule adsorbs in −S −S or −S −N(H) orientation in a bridge configuration, i.e., bridging two atomic rows of copper and involving 2, 3, or 4 Cu surface atoms[23]. On the

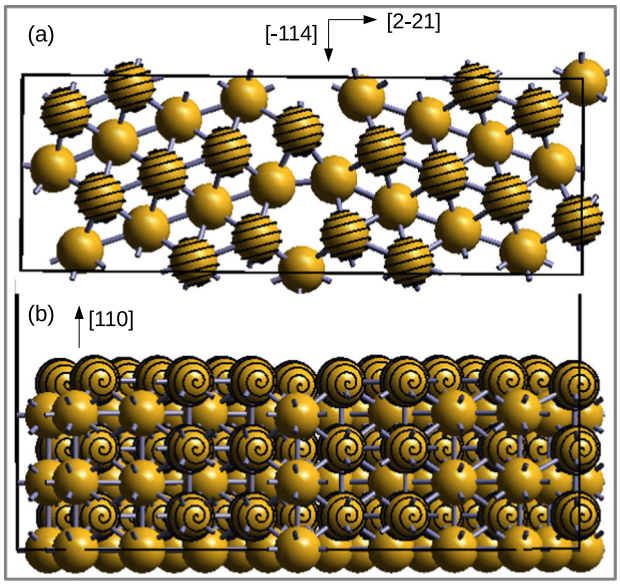

Fig. 2 Slab model of the Cu(110) bi-crystal exposing a Σ9(2$\bar{2}$1) [110] 38.9° GB. a Top view showing the two uppermost Cu(110) planes, **b** side view of the six Cu(110) planes of the slab with alternating atomic density.

bi-crystalline Cu(110) surface, these Cu atoms can belong to the grains or grain boundary. Therefore, adsorption can be (G,G), (GB,GB), or (GB,G), meaning that the molecule is bonded to two Cu atoms belonging to a grain, to the grain boundary, or to one Cu atom of the grain boundary and one Cu atom of a grain, respectively.

MBT adsorption at low monolayer density (0.61 molecule per nm^2)

We first investigated the adsorption of MBT at the monolayer density of 0.61 molecule per nm^2, i.e., at low coverage. Table 1 summarizes the adsorption energies calculated for the most stable configurations. For the MBTH thione species, the adsorption energy is around −2 eV per molecule. On the T_1 and T_2 surface terminations, the −S −S adsorption mode is slightly more stable than the −S −NH adsorption mode. This is observed for all local zones, except on T_1 GB where both orientations are iso-energetic. In contrast, for the MBT° thiolate species, the adsorption via the −S −N atoms is more stable than via the −S −S atoms on the two different GB terminations, with values of −2.33 ± 0.02 eV per molecule. These results, obtained with the thione species as reference energy, reveal that the adsorption of thiolate via the −S −N orientation is favored over the adsorption of the thione. Taking as reference the thiolate species itself, the adsorption energy (bracketed values in Table 1) is even stronger. This suggests that in the presence of both thione and thiolate forms, thiolate will adsorb preferentially at the surface, including in the GB zone.

A more detailed account of the adsorbed configurations is given in the following paragraphs, zone by zone.

Adsorption on the grain zone (G,G). Figure 4 shows the relevant, most stable configurations of the thione and thiolate forms adsorbed on the grain zone at the low monolayer density of 0.61 molecule per nm^2. Two different orientations of each species with respect to the surface are shown: thione oriented via −S −S and −S −NH in Fig. 4a, b, respectively, and thiolate oriented via −S −S and −S −N in Fig. 4c, d, respectively.

For the MBTH thione, the −S −S adsorption mode is more stable by 0.12 eV per molecule than the −S −NH adsorption mode

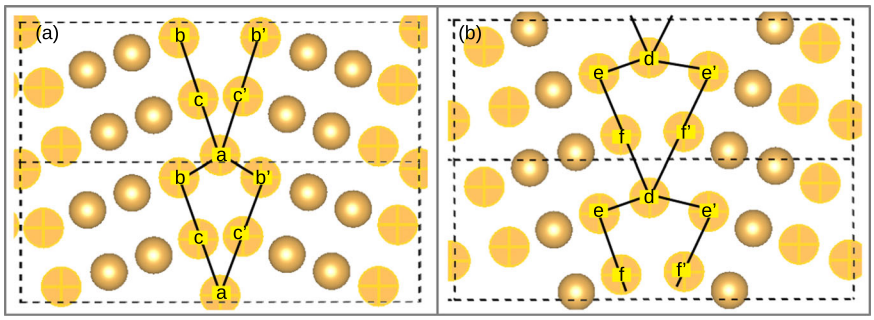

Fig. 3 Bi-crystalline Cu(110) surface exposing a Σ9(2-21)[110] 38.9° GB. Top view of the topmost plane of the T1 (**a**) and T2 (**b**) surface terminations with hatched atoms corresponding to the GB atoms. The GB sites are labeled a to c in T1 termination and d to f in T2 termination.

Table 1. Adsorption energies of the MBT thione and thiolate species at monolayer densities of 0.61 and 3.68 molecules per nm^2 on the grain (G) and grain boundary (GB) zones of the T_1 and T_2 surface terminations of the Cu(110) bi-crystal with an emergent Σ9(2$\bar{1}$1)[110] 38.9° GB.

Local adsorption zone		MBT layer density (mol per nm^2)	Thione Ads. mode	Thione E_{ads} (eV per molecule)	Thione E_{ads} (eV per nm^2)	Thiolate Ads. mode	Thiolate E_{ads} (eV per molecule)	Thiolate E_{ads} (eV/nm^2)
(G,G)		0.61	−S −S	−2.01	−1.23	−S −N	−2.35 (−3.96)	−1.43
	(GB,GB)	0.61	−S −S/−S −N	−1.98/−1.99	−1.21	−S −N	−2.31 (−3.92)	−1.41
T_1	(GB,G)	0.61	−S −S	−1.99	−1.21	−S −N	−2.38 (−3.99)	−1.45
	All zones	3.68	−S −S	−1.86	−6.84	−S −N	−2.16	−7.94
	(GB,GB)	0.61	−S −S	−2.13	−1.30	−S −N	−2.34 (−3.95)	−1.43
T_2	(GB,G)	0.61	−S −S	−1.98	−1.21	−S −N	−2.33 (−3.93)	−1.42
	All zones	3.68	−S −S	−1.85	−6.81	−S −N	−2.10	−7.73

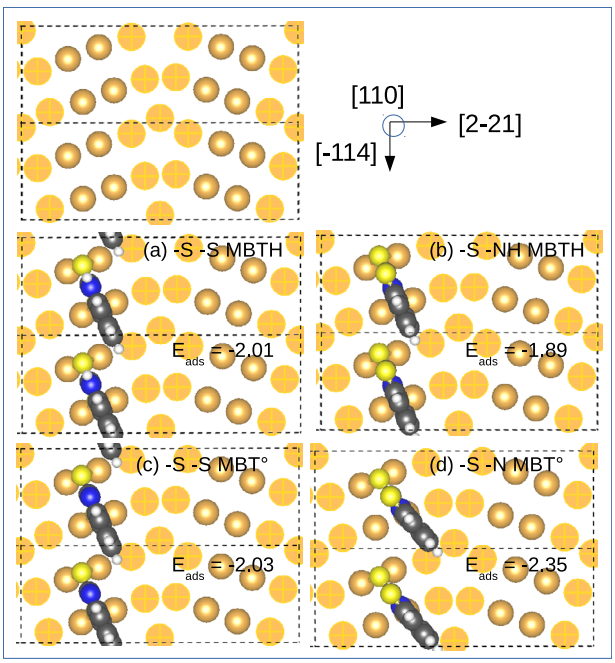

Fig. 4 Most stable configurations with their adsorption energies (in eV per molecule) of MBT adsorbed on the grain zone (G,G) of the Cu(110) bi-crystal with an emergent Σ9(2$\bar{1}$1)[110] 38.9° GB. **a** Thione via −S −S, **b** thione via −S −NH, **c** thiolate via -S -S and **d** thiolate via –S –N. Hatched atoms correspond to the GB copper atoms. Color atoms correspond to Yellow: sulfur, Blue: nitrogen, Gray: carbon, White: hydrogen.

(−2.01 and −1.89 eV per molecule, respectively). In both adsorbed configurations, the molecular plane stands perpendicular to the copper surface. In the −S −S adsorption mode, MBTH binds covalently via both sulfur atoms localized close to short bridge sites, with Cu–S_{exo}–Cu bond lengths of 2.27 and 2.32 Å and Cu–S_{endo}–Cu bond lengths of 2.23 and 2.26 Å, respectively.

For the MBT° thiolate, the −S −N adsorption mode is more stable by 0.32 eV per molecule than the −S −S adsorption mode (−2.35 and −2.03 eV per molecule, respectively). Adsorption via the −S −N orientation involves the S_{exo} and N atoms forming covalent bonds of shorter lengths with the surface Cu atoms. The Cu–S_{exo}–Cu bond lengths are 2.22 and 2.28 Å, with the S_{exo} atom localized close to a short bridge site. The N–Cu bond length is 2.01 Å, with the N atom localized on a top site. In this −S −N configuration, the molecular plane can be perpendicular or tilted to the copper surface, with the tilted adsorption being slightly more stable (0.07 eV per molecule) than the perpendicular one.

Adsorption on the grain boundary zone (GB,GB). The relevant, most stable configurations of the thione and thiolate forms adsorbed on the emergent Σ9(2$\bar{1}$1)[110] 38.9° GB at the low monolayer density of 0.61 molecule per nm^2 are shown in Fig. 5. For the T_1 surface termination, the copper atoms labeled Cu(a), Cu(b), Cu(c) and by symmetry Cu(b′) and Cu(c′) belong to the GB zone, while for the T_2 surface termination, the Cu(d), Cu(e), Cu(f) and by symmetry Cu(e′) and Cu(f′) belong to the GB zone. This notation is used to indicate the GB Cu atoms involved in the interaction mechanism with the two MBT conformers. Panels (a) and (b) correspond to the thione adsorbed via the −S −S and −S −NH orientations, respectively. Panels (c) and (d) correspond to the thiolate adsorbed via the −S −S and −S −N orientations, respectively.

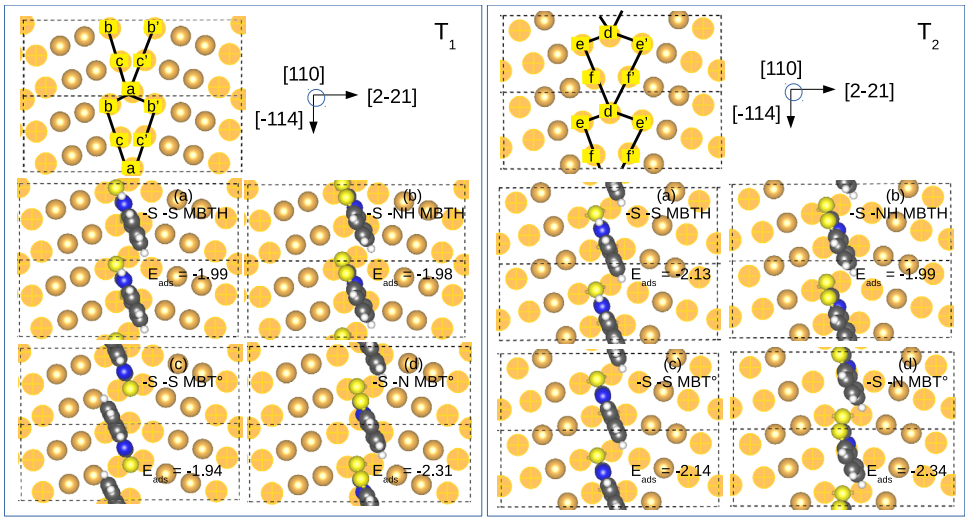

Fig. 5 Most stable configurations with their adsorption energies (in eV per molecule) of MBT adsorbed on the T_1 and T_2 terminations of the Σ9(2$\bar{2}$1)[110] 38.9° GB zone. Left: **a** thione via −S −S, **b** thione via −S −NH, **c** thiolate via −S −S, and **d** thiolate via −S −N on T_1 termination. Right: **a** thione via −S −S, **b** thione via −S −NH, **c** thiolate via −S −S, and **d** thiolate via −S −N on T_2 termination. Hatched atoms correspond to the copper atoms localized on GB zone and labeled a to f. Color atoms correspond to Yellow: sulfur, Blue: nitrogen, Gray: carbon, White: hydrogen.

The orientation of MBT adsorbed on GB zones is similar to that found on the grain surface zone. In all configurations, the thione stands perpendicular to the copper surface, whereas tilted and perpendicular adsorption configurations are energetically similar for the thiolate form. The sulfur atoms are preferentially adsorbed on short bridge GB sites, whereas the N atom or NH group are preferentially located on top or hollow copper sites, respectively.

The adsorption trends are also similar to that found on the grain zone. However, the adsorption of the thione and thiolate forms on the grain zone show one most stable configuration for each adsorption mode. In contrast, several stable configurations were found on the GB zones, involving different GB copper atoms as described below. In fact, the GB zones provide a variety of combination of adsorption sites, with close reactivity. This indicates that there is a better adaptability for the interaction between the GB atoms and the inhibitor molecules.

Thione@T_1(GB,GB): On the T_1 GB termination (Fig. 5(Left)), the most stable configuration of the −S −S adsorption mode of the thione has both sulfur atoms localized on short bridge surface sites of the GB zone. The copper sites involved in the formation of the covalent bonds are the Cu(a) and Cu(b) atoms with the S_{exo} atom and the symmetric Cu(c) and Cu(c′) atoms with the S_{endo} atom, (Fig. 5(Left)(a)). However, other combinations involving different GB atoms in the interaction are possible and iso-energetic, with an adsorption energy of about −2 eV per molecule: a configuration where Cu(a) and Cu(b) bind to S_{endo} and symmetric Cu(c) and Cu(c′) bind to S_{exo} atom, a configuration where Cu(a) and Cu(b′) bind to S_{exo} and symmetric Cu(c) and Cu(c′) bind to S_{endo} and a configuration where Cu(a) and Cu(b′) bind to S_{endo} and symmetric Cu(c) and Cu(c′) bind to S_{exo}. The Cu–S_{exo}–Cu bond lengths are 2.27 and 2.31 Å and the Cu–S_{endo}–Cu bond lengths are 2.26 and 2.29 Å. For the most stable −S −NH adsorption configuration, similar GB copper atoms are bonded to the S_{exo} atom, as it can be seen in the example depicted in Fig. 5(Left)(b) for which the adsorption energy is similar to that of the −S −S adsorption mode. The S_{exo} atom can be accommodated on short bridge sites involving Cu(a) and Cu(b), Cu(a) and Cu(b′) or Cu(c) and Cu(c′) GB atoms, with Cu–S_{exo}–Cu bond lengths of 2.30 and 2.33 Å. For all configurations, the NH group is localized on hollow sites close to the surface at a distance of about 1.18 Å, which contributes to the interaction mechanism by electrostatic interactions.

Thiolate@T_1(GB,GB): Thiolate adsorption on the T_1 GB termination exhibits more versatility than on the grain zone. The molecule can chemisorb in several iso-energetic stable configurations via the −S −N atoms, with an adsorption energy of −2.31 (−3.92) eV per molecule, which is more stable by 0.31 eV per molecule than adsorption via the −S −S atoms. MBT° thiolate binds covalently via the S_{exo} and N atoms localized close to short bridge and on top sites, respectively. The GB copper atoms involved in the interaction with the molecule are the symmetric Cu(c) and Cu(c′) sites with the S_{exo} atom and the Cu(a) site with the N atom for the configuration shown in Fig. 5(Left)(d). The Cu–S_{exo}–Cu bond lengths are 2.20 and 2.32 Å, and the N–Cu bond length is 2.01 Å. Other stable, iso-energetic configurations involve Cu(a) and Cu(b) with S_{exo} and Cu(c′) with N atoms, Cu(a) and Cu(b′) with S_{exo} and Cu(c) with N atoms, and Cu(c) and Cu(c′) with S_{exo} and Cu(b) (or symmetric Cu(b′)) site with N atoms.

Thione@T_2(GB,GB): On the T_2 GB termination (Fig. 5(Right)), the adsorption energy of the thione form is slightly lower (stronger adsorption) than on the grain zone, by 0.12 eV per molecule for the −S −S adsorption mode. The −S −S configuration is more stable by 0.14 eV per molecule than the −S −NH one. We calculated an adsorption energy of −2.13 and −1.99 eV per molecule for the −S −S and −S −NH adsorption modes, respectively. The S_{exo} atom binds to Cu(d) and Cu(e) (or symmetric Cu(e′)) atoms in short bridge site and the S_{endo} binds in close to short bridge site involving symmetric Cu(f) and Cu(f′) atoms as illustrated by an example in Fig. 5(Right)(a). The Cu–S_{exo}–Cu bond lengths are 2.29 and 2.30 Å, and the Cu–S_{endo}–Cu bond lengths are 2.29 and 2.37 Å. Similar GB copper atoms are bonded to the S_{exo} atom in the −S −NH adsorption mode with an example shown in Fig. 5(Right)(b). The NH group is localized close to the hollow site at a distance of 0.96 Å from the surface. The Cu–S_{exo}–Cu bond lengths are 2.30 and 2.33 Å.

Thiolate@T_2(GB,GB): On the T_2 GB termination (Fig. 5)(Right)), the adsorption energy of the thiolate is −2.14 eV per molecule for the −S −S mode and −2.34 (−3.95) eV per molecule for the −S −N mode, confirming that the thiolate form prefers the −S −N adsorption mode regardless of the surface zone and GB termination. In the −S −N orientation, the thiolate has three stable adsorption configurations, involving different GB copper atoms. MBT° binds covalently via the S_{exo} and N atoms localized close to short bridge and on top sites, respectively. The combination of copper atoms

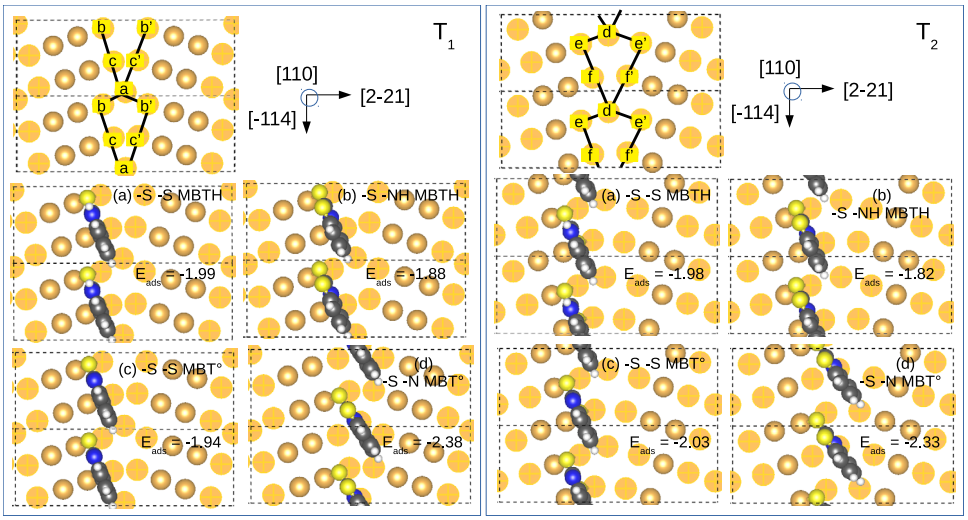

Fig. 6 Most stable configurations with their adsorption energies (in eV per molecule) of adsorbed MBT bridging Σ9(2$\bar{2}$1)[110] 38.9° GB sites and adjacent grain sites. Left: **a** thione via −S −S, **b** thione via −S −NH, **c** thiolate via −S −S, and **d** thiolate via −S −N on T_1 termination. Right: **a** thione via −S −S, **b** thione via −S −NH, **c** thiolate via −S −S, and **d** thiolate via −S −N on T_2 termination. Hatched atoms correspond to the GB copper atoms. Color atoms are Yellow: sulfur, Blue: nitrogen, Gray: carbon, White: hydrogen.

involved in the covalent bonding are the symmetric Cu(f) and Cu(f′) bridge site with the S_{exo} atom and the Cu(d) site with the N atom for the adsorption configuration shown in Fig. 5(Right)(d). The Cu–S_{exo}–Cu bond lengths are 2.22 and 2.27 Å, and the N–Cu bond length is 2.00 Å. The two other stable, iso-energetic configurations involve the Cu(d) and Cu(e) bridge site with the S_{exo} atom and the Cu(f) with N atom, and by symmetry the Cu(d) and Cu(e′) bridge site with the S_{exo} atom and Cu(f′) with N atom.

Adsorption bridging the grain boundary and grain zones. The most stable configurations for the thione and thiolate forms adsorbed at the low monolayer density of 0.61 molecule per nm^2 and bridging the Σ9(2$\bar{2}$1)[110] 38.9° GB sites and adjacent grain sites are shown in Fig. 6 for T_1 and T_2 surface terminations.

For the thione form, half of the copper atoms involved in the adsorption belong to the GB zone and the other half to the adjacent grain. For the thiolate in the −S −N adsorption mode, $\frac{2}{3}$ of copper atoms belong to the GB zone and $\frac{1}{3}$ to the adjacent grain, whereas in the −S −S orientation, half of copper atoms belong to the GB zone and the other half to the adjacent grain. The adsorption of the thione in −S −S mode being more stable than in −S −NH mode by 0.11 and 0.16 eV per molecule on the T_1 and T_2 terminations, respectively, and the adsorption of the thiolate in −S −N mode being more stable than in −S −S mode by 0.44 and 0.30 eV per molecule on the T_1 and T_2 terminations, respectively, we focus the analysis on the most stable thione and thiolate adsorption configurations only.

The results reveal similar adsorption behavior for the two terminations of the (GB,G) zone. The molecular planes stand perpendicular to the copper surface and both sulfur atoms are localized on short or close to short bridge copper sites, whereas the N atom is localized close to top copper site.

Thione@(GB,G): The adsorption energies of the thione form via its two sulfur atoms are −1.99 and −1.98 eV per molecule on the T_1 and T_2 terminations, respectively. The values reveal the strong adsorption of the species, whatever the involved zone of the surface. The adsorption involves different reactive atoms. MBTH binds covalently with Cu–S_{exo}–Cu and Cu–S_{endo}–Cu bond lengths of 2.28 (2.29) and 2.28 (2.30) Å, respectively, on the T_1 termination and 2.29 (2.30) and 2.24 (2.27) Å, respectively, on the T_2 termination.

Thiolate@(GB,G): For adsorption of the thiolate form via the −S −N orientation, we calculated an adsorption energy of −2.38 (−3.99) and −2.33 (−3.93) eV per molecule on the T_1 and T_2 terminations, respectively, considering the thione (or thiolate) form as energy reference of the molecule. MBT° binds covalently via S_{exo} on close to short bridge site, with Cu–S_{exo}–Cu bond lengths of 2.24 and 2.31 Å on the T_1 termination and 2.22 and 2.34 Å on the T_2 termination. It also forms a covalent bond via the N atom localized close to top site, with N–Cu bond lengths of 1.99 and 2.01 Å on the T_1 and T_2 terminations, respectively.

MBT adsorption at high monolayer density (3.68 molecule per nm^2)

It is interesting to investigate whether the molecules can form a full monolayer at the surface, covering simultaneously the G, GB, and the GB-G zones. This criterion is relevant for the molecules to be good corrosion inhibitors and protect the surfaces not only at grain surfaces or at the emergence of grain boundaries but uniformly. We choose a monolayer density of 3.68 molecule per nm^2 for which all copper surface atoms, belonging to the G, GB, and (GB,G) zones, are involved in the interaction with the molecules. Thus, all local zones are covered.

A wide range of configurations were constructed by combining all the possible adsorption sites identified at low monolayer density on the G, GB, and GB-G zones. The orientation of the molecules via −S −S and −S −N(NH) was also taken into account. Here we focus the analysis only on the most stable adsorption configurations and orientation of the thione and thiolate species at a monolayer density corresponding to full surface coverage. Thus, we discuss the thione adsorbed in −S −S mode and the thiolate adsorbed in −S −N mode. Indeed, calculations confirmed that the total energy difference (Δ*E*) between the −S −S and −S −N(−NH) orientations of the molecules is about 0.40 eV for both thione and thiolate species on the T_1 termination. The most stable configurations are shown in Fig. 7.

The adsorption energies of the thione form are in the same order on the T_1 and T_2 terminations, with values of −1.86 and −1.85 eV per molecule, respectively. The absolute values are inferior to those calculated at low monolayer density by 0.13 and 0.28 eV per molecule, respectively. Similar trends are found for the adsorbed thiolate form with an adsorption energy of −2.16 and −2.10 eV per molecule on the T_1 and T_2 terminations, respectively, lower in absolute values by about 0.15 and 0.24 eV per molecule compared to those calculated for low monolayer density.

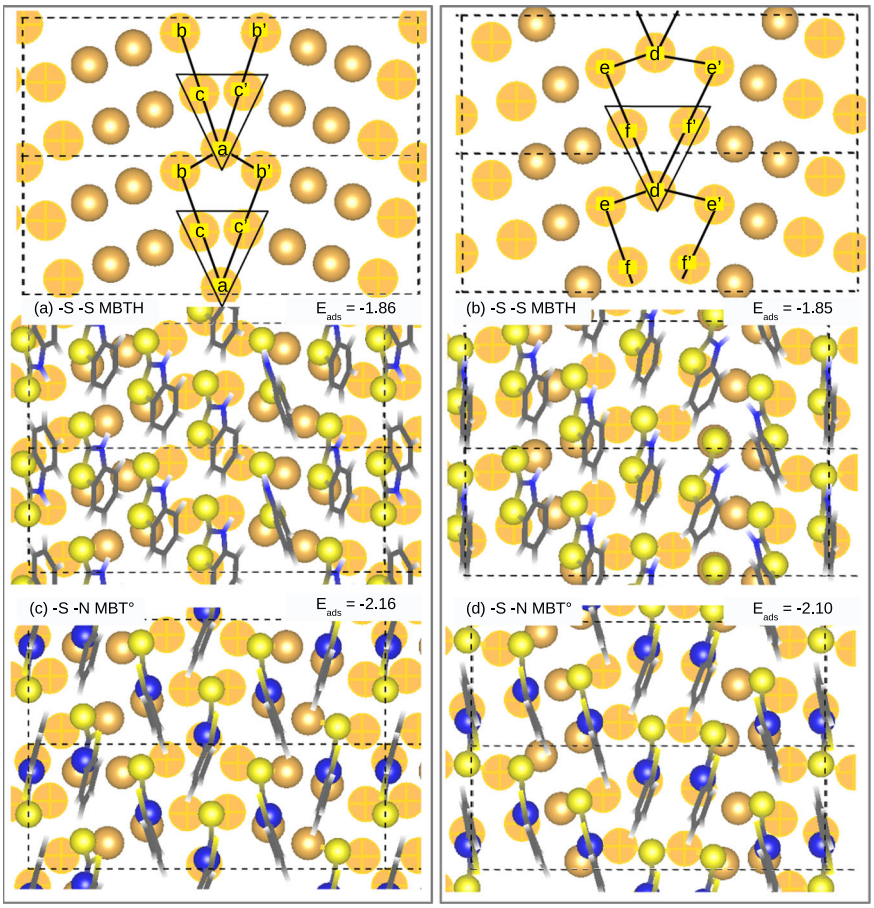

Fig. 7 Most stable thione and thiolate high density adsorption configurations on T_1 (left) and T_2 (right) terminations, with their adsorption energies (in eV per molecule). a, **b** Thione in –S –S mode, **c**, **d** thiolate in –S –N mode. Hatched Cu atoms correspond to GB atoms. Color atoms are Yellow: sulfur, Blue: nitrogen, Gray: carbon, White: hydrogen.

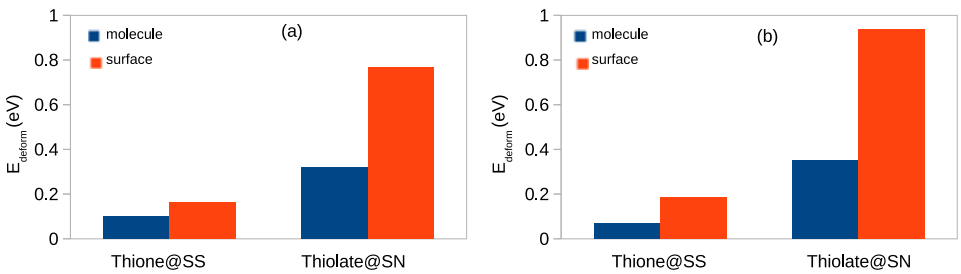

Fig. 8 Energy cost for adsorption at high monolayer density. Molecule (eV per molecule) and surface (eV per nm^2) deformation energies of thione and thiolate forms adsorbed on **a** T_1 and **b** T_2 surface terminations at high monolayer density.

Nevertheless, the normalization of the adsorption energy per unit area remains in favor of the formation of a dense organic layer for both species on the two terminations (Table 1).

The decrease (in absolute values) of the adsorption energy at full monolayer density compared to low monolayer density is due to the deformation of the molecules in the dense organic film and of the substrate surface as shown in Fig. 8. Increasing the surface coverage of the organic film from low to high molecular density increases the deformation of the surface substrate. This leads to lower (in absolute value) adsorption energy. This trend was already observed on the single-crystalline Cu(110) surface[23]. The surface deformation energy is higher for thiolate form in −S −N adsorption orientation than for the thione form in −S −S adsorption, meaning that the thiolate form loses more adsorption energy than the thione form. The molecule deformation energy varies from 0.31 to 0.37 eV per molecule for the thiolate form versus only about 0.07 eV per molecule for the thione form, regardless of surface coverage and involved surface zone. In contrast, the surface deformation energy is almost similar for both species. At low monolayer density, it varies from 0.05 to 0.10 eV per nm^2, according to the adsorption zones and surface termination, while at high monolayer density, values can reach 0.18 eV per nm^2 for the thione form and 0.94 eV per nm^2 for the thiolate form on the T_2 termination.

The most stable arrangement of the molecules on the T_1 termination (Fig. 7(left)) shows that the molecule adsorbed on GB zone is located on a small triangle formed by the two symmetric Cu(c) and Cu(c') sites and the Cu(a) site (see Fig. 7 (top left)). The

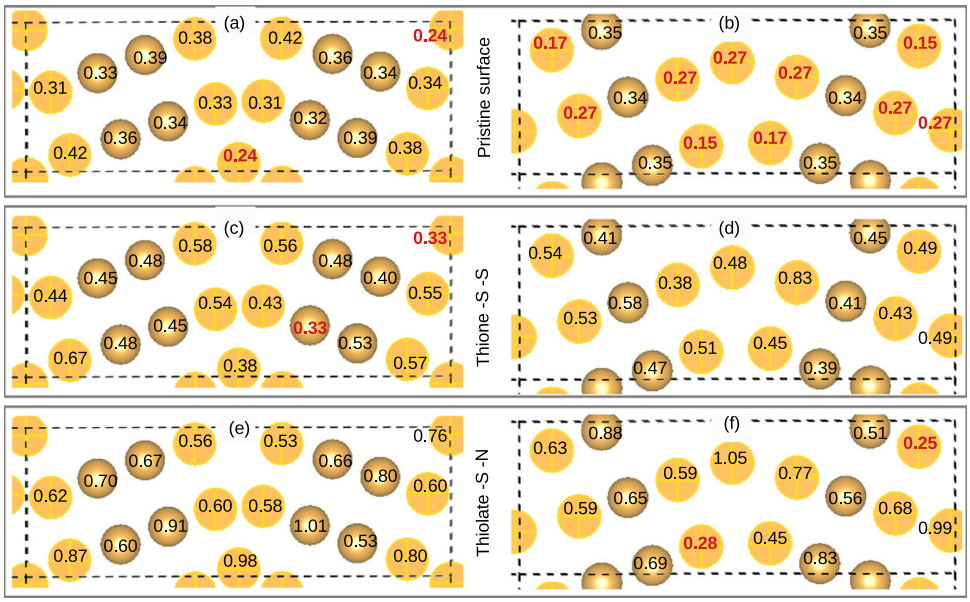

Fig. 9 Values of Cu vacancy formation energy (eV per atom) for the different copper sites of the bi-crystalline Cu(110) surface exposing an emergent Σ9(2$\bar{2}$1)[110] 38.9° GB. a T_1 termination, bare surface; **b** T_2 termination, bare surface; **c** T_1 termination, thione-covered surface; **d** T_2 termination, thione-covered surface; **e** T_1 termination, thiolate-covered surface; **f** T_2 termination, thiolate-covered surface. Values in red mark more reactive copper sites.

molecule binds covalently via the S_{exo} atom on short bridge site over the Cu(c) and Cu(c') atoms. Another covalent bond is formed via the S_{endo} atom (for the thione species) or N atom (for the thiolate species) on top site over the Cu(a) atom. The molecule adsorbed in the (GB,G) zones involves one copper atom belonging to the GB zone (Cu(b) or symmetric Cu(b') site) and two copper atoms of the adjacent grain. The S_{exo} atom is localized on short bridge site, involving 1 GB atom and 1 adjacent G atom. The S_{endo} (for thione) or N (for thiolate) is localized on top site on 1 adjacent G atom.

In the most stable configuration on the T_2 termination (Fig. 7(right)), the molecule adsorbed on the GB zone is located on a small triangle formed by two symmetric Cu(f) and Cu(f') sites and Cu(d) site (see Fig. 7 (top right)). The difference between the two triangular GB site of the T_1 and T_2 terminations is in Cu–Cu bond length, which is longer on the T_2 termination due to the lower copper density. Indeed, the distance between the Cu(f) and symmetric Cu(f') sites of the T_2 termination is about 3.35 Å, and it is shorter by 0.97 Å between Cu(c) and symmetric Cu(c') sites of the T_1 termination. However, the reactivity of the molecules toward the surfaces remains strong. The molecule binds covalently on GB zone, involving the S_{exo} atom in short bridge site on the Cu(f) and Cu(f') atoms and the S_{endo} (for thione) or N (for thiolate) atom on top site over the Cu(d) atom. The molecules adsorbed on the (GB,G) zones show two adsorption configurations. The molecule can bind to one GB copper atom (Cu(e) or symmetric Cu(e') site) and two copper atoms of the adjacent grain, as observed on the T_1 termination. The molecule can also bind to only two copper atoms, one GB atom, and one adjacent G atom. The S_{exo} atom is localized on short bridge (for the molecule involving three copper atoms) or close to top (for the molecule involving two copper atoms) sites. It interacts with one GB atom and one G atom or only with one GB copper atom. The S_{endo} (for thione) or N (for thiolate) is localized on top site over the G atoms adjacent to the grain boundary.

To summarize, both forms of MBT have the ability to adsorb on the grain zone and also on the GB and (GB,G) zones at high surface coverage. The adsorption configurations are stable and the interaction remains strong, even if we observed a loss in the adsorption energy as compared to the adsorption of single molecule on each zone. The reactivity and the bonding strength of the thiolate species is greater than that of the thione species, despite the strong surface deformation induced by the adsorption of the thiolate species. The adsorbed molecules can self-assemble in different combinations, involving the GB sites and the adjacent grain sites. Each molecule can interact with 3 copper atoms on the T_1 termination and with two and three copper atoms on the T_2 termination, due to the lower density of copper atoms in the GB zone of the latter. In the GB zones, stability of the adsorbed molecule is ensured by the GB copper atoms forming small triangle, Cu(c), Cu(c'), and Cu(a) for the T_1 termination and Cu(f), Cu(f'), and Cu(d) for the T_2 termination, while in the (GB,G) zone the adsorbed molecules interacts with a GB copper atom and a copper atom of the adjacent grain.

Defect formation energy

In order to discuss the inhibiting effect of the adsorbed organic monolayer on the dissolution of the metal, we calculated, using Eq. (5), the Cu vacancy formation energy in the absence or presence of the high density monolayer (3.68 molecule per nm^2) of adsorbed MBT molecules. This quantity corresponds to the defect formation energy (E_f) for injecting one Cu vacancy localized on different grain and GB sites. Values are reported in Fig. 9 for the bare surface and for the surface covered by the organic films formed by the thione species in the −S −S adsorption mode or by the thiolate species in the −S −N adsorption mode. The results are given for both the T_1 and T_2 surface terminations.

The results obtained on the bare surfaces (Fig. 9a and b) show that the defect formation energy for one Cu vacancy depends on the local zone and that the GB sites are indeed preferential sites of dissolution since it is slightly easier to create the vacancies on the GB zones, particularly for the less dense T_2 termination. We calculated values from 0.33 to 0.39 eV per atom for the atoms localized on grain zones in line with the value of 0.33 eV per atom found on a single-crystalline Cu(110) surface[23]. On the T_1 termination (Fig. 9a), some of the GB sites show a similar defect formation energy as the grain sites, like the Cu(b), Cu(c) and their symmetric sites. The most sensitive GB site for dissolution is the

Cu(a) atom, with a defect formation energy of 0.24 eV per atom. On the T_2 termination (Fig. 9b), we calculated a GB defect formation energy lower than on the grains, with values varying from 0.15 to 0.27 eV per atom for the different GB sites. These values are low, meaning that the copper sites of the GB zone of lower atomic density are more sensitive to dissolution. The results show that the emergent GB is indeed a local zone of favored Cu dissolution compared to adjacent grains and that our model is adequate to study the effects of adsorbed corrosion inhibitors.

In the presence of full monolayer of organic molecules, we calculated a higher defect formation energy than for the bare surface for the different zones (grain and GB sites). The results show that both conformers of MBT have the ability to enhance the Cu bonding strength. For the T_1 termination and according to the surface zone and involved copper site, the defect formation energy varies from 0.33 to 0.67 eV per atom in the presence of the thione monolayer (Fig. 9c), and from 0.53 to 1.01 eV per atom in the presence of the thiolate monolayer (Fig. 9e). For the T_2 termination, the defect formation energy varies from 0.39 to 0.83 eV per atom with the adsorbed thione monolayer (Fig. 9d) and from 0.51 to 1.05 eV per atom with the adsorbed thiolate monolayer (Fig. 9f). We can observe that in contrast to the bare surface, the vacancy formation energies are unsymmetrical in the presence of the molecules. In fact, the adsorption of the molecules breaks the GB symmetry, as the symmetrical surface sites do not systematically bind with the same molecule fragment. Indeed, we observed that the molecules slightly reorient in order to adapt to the orientation change. In addition, molecule adsorption on the grain near the GB breaks the GB symmetry.

For the different zones, the protection against dissolution of the Cu atoms is stronger in the presence of the thiolate monolayer than in the presence of the thione monolayer. However, for the thione-covered T_1 termination (Fig. 9c), some copper atoms of the GB zone remain as sensitive to dissolution as on the bare surface with almost the same defect formation energy (0.33 eV per atom). Similar observations can be made for the thiolate-covered T_2 termination (Fig. 9f). In this latter case, we even note that two Cu sites are slightly more sensitive to the extraction than on the bare grain zone, with a defect formation energy of 0.25 and 0.28 eV per atom, but they are enhanced compared to the bare GB zone, where the defect formation energy is 0.15 eV per atom. These results evidence that the inhibition of the Cu dissolution by the adsorbed organic monolayers may not reach 100% efficiency at the emergence of a grain boundary. For the thione-covered T_1 termination, the copper atoms interacting with the S_{exo} atoms have their stability more enhanced, by about 0.10 eV, than the copper atoms involved with S_{endo} atoms. In contrast, for both thiolate-covered terminations, all copper sites interacting with the S_{exo} and N atoms have a higher defect formation energy (Fig. 9e and f) compared to bare surfaces. Therefore, the thiolate species provides a better protection of the surface against dissolution of the copper atoms than the thione species.

It has been recently shown that at the emergence of high Σ CSL GB, MBT does not fully inhibit local dissolution nor the formation of a Cu(I) passivating oxide as evidenced by the accumulation of reaction products[1,24]. Our results confirm that Cu dissolution is not hindered for 12% of the surface sites at the emergence of a Σ9 CSL GB. A possible scenario is that a multilayer of MBT is formed at the surface, as evidenced by XPS measurements[17,33]. The Cu atoms which extraction is not hindered have a high probability to bind with a MBT molecule in the layers above the first, strongly chemisorbed layer. In other words, the role of the first MBT layer would be: (i) to inhibit the entry of aggressive species, (ii) to enhance the energy required for Cu extraction and thus decrease the dissolution probability, and iii) to serve as an anchoring layer for multi-layers that are a reservoir of molecules for the formation of complexes with the Cu atoms extracted from the surface.

A last comment concerns the ability of MBT to preclude Cu(I) oxide formation and thus passivation. This can be examined by comparing the binding energies of MBT and OH with the surface. Dissociative water adsorption on the Cu(110) surface is reported to be −0.63 eV/H_2O[34]. MBT adsorption energy at high monolayer density is −1.8/−1.9 eV per molecule (thione) and −2.1/−2.2 eV per molecule (thiolate). As MBT binds to two Cu atoms, we have to compare its adsorption energy with that of two water molecules, that is −1.26 eV. This comparison suggests that MBT adsorption is always favored over water adsorption, and thus may block the dissociative adsorption of water at the origin of Cu(I) oxide formation.

Our results show that the adsorption of MBT on a Cu(110) bi-crystal exposing a Σ9 GB is exothermic, and that MBT can cover the whole surface including the emergent GB thus forming a monolayer with a high density of 3.68 mol/nm^2, as on the surface of the Cu(110) single-crystal. The thiolate adsorption is favored over thione adsorption. In the presence of the adsorbed organic monolayer, the energy required for Cu extraction is high compared to that calculated for the bare surface. However, some Cu sites on GBs remain susceptible to the dissolution even in the presence of organic molecules, with similar energy of Cu extraction than on the bare surface. The present calculations are useful to rationalize and understand recent experimental data. In particular, it is shown here that most of surface Cu atoms increase their binding energy with the surface, and thus are less prompt to dissolution in the presence of a high density MBT monolayer. The persistence of a fraction of Cu atoms that do not have an increased binding energy with the surface, and thus remain susceptible to dissolution, explains the experimentally observed accumulation of complexes at high Σ CSL GBs.

METHODS

Computational details

All calculations were performed using the framework of DFT with the periodic plane-wave basis set implemented in the Vienna Ab initio Simulation Package (VASP)[35,36]. Energy analysis for the reported minimized structures was obtained with projector-augmented-wave potentials[37,38]. Electron exchange and correlation terms were treated within the general gradient approximation (GGA) of the Perdew-Burke-Ernzehof (PBE) functional[39,40]. For all calculations, the plane-wave energy cutoff was 450 eV and a Methfessel-Paxton smearing[41] with smearing value of 0.1 eV was used. Atomic positions were relaxed with the conjugate gradient (CG) algorithm until forces on each moving atom were less than 0.02 eV Å^{-1}. The van der Waals contributions were considered in the Grimme D2 empirical dispersion correction[42], giving a good compromise for the lattice parameters of bulk copper metal with equilibrium values of 3.57 Å, obtained using a 21 × 21 × 21 k-mesh and in good agreement with experimental and calculated PBE values of 3.61[43] and 3.57 Å[44], respectively.

The Brillouin zone sampling was set to a 3 × 1 × 1 k-mesh[45] for the bare surfaces and molecule/surface systems. The vacuum region was set at more than 18 Å to minimize the interactions in the *z* direction between periodic images of the system. All calculations were done without any constraint on the structure, except for the three bottom layers of the slab (asymmetric slab). The three upmost metal layers and the molecules were let free to relax.

The isolated molecules were optimized using the same computational conditions, except for the Brillouin zone sampling restricted to the Γ-point, in a box with large dimensions of 20 × 20 × 20 Å in the three directions. For the radical MBT° form, spin polarization was implemented to get the energy minimum.

Energy analysis

The adsorption energy of the MBT molecule for the thione (MBTH) and thiolate (MBT°) forms was calculated as:

$$E_{ads} = [E(\text{slab/n-MBT}) - E(\text{slab}) - nE(\text{MBT})]/n \quad (1)$$

where E(slab/n-MBT) is the total energy of the system with MBTH or MBT° adsorbed on the surface. E(slab) and E(MBT) are the energies for the bare relaxed surface and the free MBTH or MBT° species optimized in vacuum, respectively. n is the number of molecules on the surface. For the thiolate (MBT°) form, the adsorption energy was also calculated, considering the thione form as the energy reference:

$$E_{ads} = [E(\text{slab/n-MBT}^{\circ}) + \frac{n}{2}E(H_2) - E(\text{slab}) - nE(\text{MBTH})]/n \quad (2)$$

where E(slab/n-MBT°) is the total energy of the system with MBT° adsorbed on the surface from MBTH. $E(H_2)$ is the energy of the released H_2 molecule, optimized in vacuum.

The surface deformation energy of the slab was calculated as:

$$E_{deform} = E^{urlx}(\text{slab}) - E(\text{slab}) \quad (3)$$

where E^{urlx}(slab) is the energy of the unrelaxed free slab obtained after separation from the adsorbed molecules.

The deformation energy per molecule in the adsorbed organic layer was calculated as:

$$E_{deform} = E^{urlx}(\text{MBT}) - E(\text{MBT}) \quad (4)$$

where E^{urlx}(MBT) is the energy of one unrelaxed molecule obtained after separation from the substrate.

In order to show the ability of MBT inhibitor to slow down the corrosion of the copper surface, we calculated the defect formation energy corresponding to the creation of one copper vacancy in the topmost copper plane in the presence and the absence of the inhibitor. The defect formation energy was calculated as:

$$E_f = E_{defect}(\text{slab/n-MBT}) + E(\text{Cu}) - E_{perfect}(\text{slab/n-MBT}) \quad (5)$$

where E_{defect}(slab/n-MBT) and $E_{perfect}$(slab/n-MBT) are the total energy of the defect and perfect surfaces, respectively. E(Cu) is the energy of bulk copper. Despite being a very simplified description of the dissolution reaction, this parameter is convenient, easy to calculate, and a relevant indicator of local corrosion susceptibility.

DATA AVAILABILITY

The data that support the findings of this study are available from the corresponding author upon reasonable request.

Received: 17 September 2022; Accepted: 10 December 2022;
Published online: 13 January 2023

REFERENCES

1. Sharma, S. B., Maurice, V., Klein, L. H. & Marcus, P. Local inhibition by 2-mercaptobenzothiazole of early stage intergranular corrosion of copper. *J. Electrochem. Soc.* **167**, 162504 (2020).
2. Bettayeb, M. et al. Nanoscale intergranular corrosion and relation with grain boundary character as studied in situ on copper. *J. Electrochem. Soc.* **165**, C835–C841 (2018).
3. A. Fateh, M. A. & Rezvanian, A. R. Review of corrosive environments for copper and its corrosion inhibitors. *Arab. J. Chem.* **13**, 481–544 (2020).
4. Ohsawa, M. & Suetaka, W. Spectro-electrochemical studies of the corrosion inhibittion of copper by 2-mercaptobenzothiazole. *Corros. Sci.* **19**, 709–722 (1979).
5. Chadwick, D. & Hashemi, T. Electron spectroscopy of corrosion inhibitors: surface films formed by 2-mercaptobenzothiazole and 2-mercaptobenzimidazole on copper. *Surf. Sci.* **89**, 649–659 (1979).
6. Marconato, J. C. & Bulho, L. O. A spectroelectrochemical study of the inhibition of the electrode process on copper by 2- mercaptobenzothiazole in ethanolic solutions. *Electrochim. Acta* **43**, 771–780 (1998).
7. Ramírez-Cano, J. A., Veleva, L., Souto, R. M. & Fernández-Pérez, B. M. SECM study of the pH distribution over Cu samples treated with 2-mercaptobenzothiazole in NaCl solution. *Electrochem. commun.* **78**, 60–63 (2017).
8. He, D., Chen, F., Chen, J., Yao, S. & Wei, W. Real-time bulk acoustic wave studies of the inhibition behavior of mercaptobenzothiazole on copper. *Thin Solid Films* **352**, 234–238 (1999).
9. Shahrabi, T., Tavakholi, H. & Hosseini, M. G. Corrosion inhibition of copper in sulphuric acid by some nitrogen heterocyclic compounds. *Anti Corros. Methods Mater.* **54**, 308–313 (2007).
10. Kazansky, L. P., Selyaninov, I. A. & Kuznetsov, Y. I. Adsorption of 2-mercaptobenzothiazole on copper surface from phosphate solutions. *Appl. Surf. Sci.* **258**, 6807–6813 (2012).
11. Chen, Y.-H. & Erbe, A. The multiple roles of an organic corrosion inhibitor on copper investigated by a combination of electrochemistry-coupled optical in situ spectroscopies. *Corros. Sci.* **145**, 232–238 (2018).
12. Woods, R., Hope, G. A. & Watling, K. A SERS spectroelectrochemical investigation of the interaction of 2-mercaptobenzothiazole with copper, silver and gold surfaces. *J. Appl. Electrochem.* **30**, 1209–1222 (2000).
13. Tan, Y. S., Srinivasan, M. P., Pehkonen, S. O. & Chooi, S. Y. M. Self-assembled organic thin films on electroplated copper for prevention of corrosion. *J. Vac. Sci. Technol. A* **22**, 1917 (2004).
14. Bao, Q., Zhang, D. & Wan, Y. 2-mercaptobenzothiazole doped chitosan/11-alkanethiolate acid composite coating: Dual function for copper protection. *Appl. Surf. Sci.* **257**, 10529–10534 (2011).
15. Li, J., Du, C. W., Liu, Z. Y., Li, X. G. & Liu, M. Inhibition film formed by 2-mercaptobenzothiazole on copper surface and its degradation mechanism in sodium chloride solution. *Int. J. Electrochem. Sci.* **11**, 10690–10705 (2016).
16. Grekulović, V., Vujasinović, M. R. & Mitovski, A. Electrochemical behavior of AgCu50 in alkaline media in the presence of clorides and 2-mercaptobenzothiazole. *J. Min. Metall. Sect. B Metall* **53**, 349–356 (2017).
17. Wu, X., Wiame, F., Maurice, V. & Marcus, P. Molecular scale insights into interaction mechanisms between organic inhibitor film and copper. *npj Mater. Degrad.* **5**, 22 (2021).
18. Chiter, F., Costa, D., Maurice, V. & Marcus, P. DFT investigation of 2-mercaptobenzothiazole adsorption on model oxidized copper surfaces and relationship with corrosion inhibition. *Appl. Surf. Sci.* **537**, 147802 (2021).
19. Vernack, E., Costa, D., Tingaut, P. & Marcus, P. DFT studies of 2-mercaptobenzothiazole and 2-mercaptobenzimidazole as corrosion inhibitors for copper. *Corros. Sci.* **174**, 108840 (2020).
20. Chiter, F., Costa, D., Maurice, V. & Marcus, P. Corrosion inhibition of locally depassivated surfaces by DFT study of 2-mercaptobenzothiazole on copper. *npj Mater. Degrad.* **5**, 52 (2021).
21. Chiter, F., Costa, D., Maurice, V. & Marcus, P. Adsorption of 2-mercaptobenzimidazole corrosion inhibitor on copper: DFT study on model oxidized interfaces. *J. Electrochem. Soc.* **167**, 161506 (2020).
22. Chiter, F., Costa, D., Maurice, V. & Marcus, P. Atomic scale insight into corrosion inhibition: DFT study of 2- mercaptobenzimidazole on locally de-passivated copper surfaces. *J. Electrochem. Soc.* **168**, 121507 (2021).
23. Chiter, F., Costa, D., Maurice, V. & Marcus, P. Chemical interaction, self-ordering and corrosion inhibition properties of 2-mercaptobenzothiazole monolayers: DFT atomistic modelling on metallic copper. *Corros. Sci.* **209**, 110658 (2022).
24. Sharma, S. B., Maurice, V., Klein, L. H. & Marcus, P. Local effects of organic inhibitor molecules on passivation of grain boundaries studied in situ on copper. *J. Electrochem. Soc.* **168**, 061501 (2021).
25. Wang, H. et al. DFT study of imidazoles adsorption on the grain boundary of Cu(100) surface. *Corros. Sci* **137**, 33–42 (2018).
26. Ni, C., Ding, H., Asta, M. & Jin, X. Computational study of $<1\bar{1}00>$ symmetric tilt grain boundaries in Mg and Ti. *Scr. Mater.* **109**, 94–99 (2015).
27. Sun, X.-Y., Taupin, V., Fressengeas, C. & Cordier, P. Continuous description of the atomic structure of grain boundaries using dislocation and generalized-disclination density fields. *Int. J. Plast.* **77**, 75–89 (2016).
28. Razumovskiy, V. I., Lozovoi, A. Y. & Razumovskii, I. M. First-principles-aided design of a new Ni-base superalloy: Influence of transition metal alloying elements on grain boundary and bulk cohesion. *Acta Mater.* **82**, 369–377 (2015).
29. Lousada, C. M. & Korzhavyi, P. A. Segregation of p and s impurities to a Σ9 grain boundary in Cu. *Metals.* **10**, 1362 (2020).
30. Mishin, O. V., Gertsman, V. Y. & Gottstein, G. Distributions of orientations and misorientations in hot-rolled copper. *Mater. Charact.* **38**, 39–48 (1997).
31. Hallberg, H. & Olsson, P. A. T. Investigation of microstructure evolution during self-annealing in thin Cu films by combining mesoscale level set and ab initio modeling. *J. Mech. Phys. Solids.* **90**, 160–178 (2016).

32. Korolev, V. V., Kucherinenko, Y. V., Makarevich, A. M., Straumal, B. B. & Protsenko, P. V. Statistics of gb misorientations in 2d polycrystalline copper foil. *Mater. Lett.* **196**, 377–380 (2017).
33. Finšgar, M. & Merl, D. K. An electrochemical, long-term immersion, and XPS study of 2-mercaptobenzothiazole as a copper corrosion inhibitor in chloride solution. *Corros. Sci.* **83**, 164–175 (2014).
34. Ren, J. & Meng, S. First-principles study of water on copper and noble metal (110) surfaces. *Phys. Rev. B.* **77**, 054110 (2008).
35. Kresse, G. & Furthmüller, J. Efficiency of ab-initio total energy calculations for metals and semiconductors using a plane-wave basis set. *Comput. Mater. Sci* **6**, 15–50 (1996).
36. Kresse, G. & Hafner, J. Ab initio molecular-dynamics simulation of the liquid-metal-amorphous-semiconductor transition in germanium. *Phys. Rev. B.* **49**, 14251–14269 (1994).
37. Kresse, G. & Joubert, D. From ultrasoft pseudopotentials to the projector augmented-wave method. *Phys. Rev. B* **59**, 1758–1775 (1999).
38. Blöchl, P. E. Projector augmented-wave method. *Phys. Rev. B* **50**, 17953 (1994).
39. Perdew, J. P. et al. Atoms, molecules, solids, and surfaces: applications of the generalized gradient approximation for exchange and correlation. *Phys. Rev. B* **46**, 6671–6687 (1992).
40. Perdew, J. P., Burke, K. & Ernzerhof, M. Generalized gradient approximation made simple. *Phys. Rev. Lett.* **77**, 3865 (1996).
41. Methfessel, M. & Paxton, A. T. High-precision sampling for Brillouin-zone integration in metals. *Phys. Rev. B* **40**, 3616 (1989).
42. Grimme, S. Semiempirical GGA-type density functional constructed with a long-range dispersion correction. *J. Comput. Chem.* **27**, 1787–1799 (2006).
43. Kittel, C. *Introduction to Solid State Physics*, 7th edn. (Wiley Sons, 1996).
44. Chiter, F. et al. Effect of van der waals corrections on DFT-computed metallic surface properties. *Mater. Res. Express* **3**, 046501 (2016).
45. Monkhorst, H. J. & Pack, J. D. Special points for Brillonin-zone integrations. *Phys. Rev. B* **13**, 5188 (1976).

ACKNOWLEDGEMENTS

This project has received funding from the European Research Council (ERC) under the European Union's Horizon 2020 research and innovation program (ERC Advanced Grant No. 741123, Corrosion Initiation Mechanisms at the Nanometric and Atomic Scales: CIMNAS). We thank GENCI for high performance calculations in the national (CINES) center under the A0040802217.

AUTHOR CONTRIBUTIONS

F.C.: Methodology, validation, investigation, formal analysis, visualization, writing—original draft, writing—review editing. D.C.: Resources, supervision, writing—review editing. V.M.: Supervision, writing—review, editing, funding acquisition. P.M.: Supervision, writing—review and editing, funding acquisition, project management.

COMPETING INTERESTS

The authors declare no competing interests.

ADDITIONAL INFORMATION

Correspondence and requests for materials should be addressed to Fatah Chiter, Vincent Maurice or Philippe Marcus.

Reprints and permission information is available at http://www.nature.com/reprints

Publisher's note Springer Nature remains neutral with regard to jurisdictional claims in published maps and institutional affiliations.